Histol Histopathol (2021) 36: 1155-1167

http://www.hh.um.es

Histology and Histopathology
From Cell Biology to Tissue Engineering

ORIGINAL ARTICLE **Open Access**

Death-associated protein kinase 1 correlates with podocyte apoptosis and renal damage and can be mediated by miR-361

Guang-jun Wu[1], Hong-biao Zhao[2] and Xiao-wei Zhang[3]

[1]Department of Traditional Chinese Medicine, [2]Department of Peripheral Vascular and [3]Department of Nephrology, Linyi Central Hospital, Linyi City, Shandong Province, China

Summary. Background. Herein, we aimed to determine whether DAPK1 and its post-transcriptional regulator miR-361 were implicated in high glucose (HG)-induced podocyte injury and renal damage in db/db mice.

Materials and methods. Podocytes were incubated with normal glucose (NG; 5 mM) or HG (30 mM). Podocyte apoptosis was evaluated using TUNEL staining. Lentiviral-delivered specific short hairpin RNA (shRNA) was designed to silence DAPK1 expression in podocytes. miR-361 agomir was administrated by tail intravenous injection in db/db diabetic mice to investigate the renoprotection of miR-361 *in vivo*.

Results. Exposure of podocytes to HG led to a significant increase in DAPK1 mRNA and protein levels and a decrease in miR-361 expression levels. Knockdown of DAPK1 attenuated HG-triggered growth inhibition, apoptosis, DNA damage and cell membrane damage in podocytes. Mechanically, DAPK1 was a direct target of miR-361. Transfection with miR-361 mimics into podocytes resulted in a significant decrease in the DAPK1 protein expression level. In addition, HG-induced the up-regulation of the DAPK1 protein expression level in podocytes was restrained by miR-361 mimics transfection. Intriguingly, overexpression of DAPK1 in HG-stimulated podocytes muted miR-361-mediated cytoprotection, including anti-apoptosis, resistance to DNA and membrane damage. *In vivo*, overexpression of miR-361 protected against hyperglycemia-induced podocyte loss, tubular atrophy and interstitial fibrosis in the kidney of db/db mice. Moreover, overexpression of miR-361 inhibited the protein expression of DAPK1 in the kidney of db/db mice.

Conclusion. Our research presented a novel mechanism of HG-induced podocyte damage or renal lesion, supporting the miR-361/DAPK1 signaling pathway that could be used as a potential therapeutic target for the treatment of DN.

Key words: miR-361, DAPK1, Podocyte, High glucose, Apoptosis

Corresponding Author: Dr. Xiao-wei Zhang, Department of Nephrology; Linyi Central Hospital, No.17 Jiankang Road, Linyi City 276400, Shandong Province, China. e-mail: pp_zhang11@21cn.com

DOI: 10.14670/HH-18-358

Introduction

Diabetic nephropathy (DN) as one of the most common microvascular complications in the progression of diabetes mellitus is a major pathogenic factor of end-stage renal disease (ESRD), which is characterized by reduced glomerular filtration rate (GFR), glomerulosclerosis and tubulointerstitial fibrosis (Roscioni et al., 2014; Chen et al., 2018). Accumulating evidence corroborates that podocyte dysfunction and damage in response to hyperglycemia stimulation contribute to microalbuminuria, which is the earliest clinical manifestation of DN, and subsequent loss of kidney function and GFR (Dai et al., 2017; Zhan et al., 2018). Nevertheless, increasing evidence substantiates that multiple signaling pathways, including adenosine monophosphate-activated kinase signaling pathways, wnt/β-catenin and mammalian target of rapamycin/autophagy pathway, are implicated in the process of podocyte depletion (Dai et al., 2017). However, the molecular mechanisms underlying high glucose-triggered podocyte dysfunction and renal damage have not been completely elaborated.

Death-associated protein kinase 1 (DAPK1) is a member of the serine/threonine kinases family and is imperative for a wide range of pathological processes, including inhibition of cancer growth, neurodegeneration and autophagy (Singh et al., 2016). Of interest, DAPK1 is also identified as a pro-apoptotic mediator of multiple cell death, including cancer cells, neuronal cells,

neutrophil and epithelial cells (Thongchot et al., 2018; Zhou et al., 2018; Cui et al., 2019). However, up to now, its function and underlying molecular mechanism remain elusive in podocyte apoptosis and renal damage.

microRNAs (miRs) play vital roles by means of binding with the 3'-untranslated region (3'-UTR) of the target gene to degrade mRNA or post-transcriptionally repress its protein translation (Baek et al., 2008). Accumulating research highlights miRs as the potential targets for the treatment of various diseases, including DN. For example, miR-23b mitigates albuminuria and renal fibrosis in a mouse model of diabetic nephropathy via repressing Ras GTPase-activating protein SH3 domain-binding protein 2 (Zhao et al., 2016). Simultaneously, miR-23b expression is inhibited in cultured kidney cells exposed to high glucose (Zhao et al., 2016). Overexpression of miR-29a elevates nephrin levels, improves podocyte homeostasis and renal function, and alleviates glomerular fibrosis and inflammation reaction in diabetic mice (Lin et al., 2014). In the present study, our results revealed that miR-361 had the ability to attenuate high glucose-evoked podocyte dysfunction and renal pathological change, including growth inhibition, apoptosis, DNA damage, cell membrane damage, tubular atrophy and interstitial fibrosis. miR-361 is validated as a multifunctional gene that is implicated in inflammation, cell apoptosis, cognitive impairment and tumorigenesis via mediating multiple target genes (Mendes-Silva et al., 2016; Xu and Dong, 2019; Huang et al., 2020). However, the biological effects of miR-361 on high glucose-induced podocyte and renal injuries are still unclear. Furthermore, we further determined whether miR-361 could target DAPK1 to improve high glucose-potentiated podocyte injury and renal damage.

Materials and methods

Cell culture

Mouse renal podocytes (cat. no: 3111C0001CCC000230) were obtained from the National Infrastructure of Cell Line Resource (http://www.cellresource.cn; Beijing, China). Differentiated podocytes were maintained in RPMI-1640 (Invitrogen, USA) containing high glucose (HG, 30 mM D-glucose) or normal glucose (NG, 5 mM D-glucose) supplemented with 10% FBS (Invitrogen, Thermo Fisher Scientific, Inc., USA) at 37°C in a humidified incubator (Thermo Fisher Scientific, Inc., USA), 5% CO_2, 95% air atmosphere.

Cell viability measurement

The cell counting kit-8 (CCK-8) proliferation assay (Dojindo, Japan) was used to evaluate cell viability in response to HG or DAPK1 knockdown as previously described (Liang et al., 2017).

TUNEL assay

After exposure to podocytes with high glucose, cell apoptosis was evaluated using TUNEL (Beyotime Institute of Biotechnology, Haimen, China) assay according to the manufacturer's instructions. TUNEL positive cells were mounted under a fluorescence microscope (BX53, Olympus, Japan; magnification, 200x). In brief, cells were fixed with 4% paraformaldehyde for 15 min at room temperature. The nerve cells were stained with TUNEL (50 μL) at 37°C for 60 min. Subsequently, cells were incubated with 100 μL DBA (0.5 mg/mL) at room temperature for 15 min. Cell nuclei were stained with hematoxylin staining solution (1%) at room temperature for 5 sec.

Cell transfection

sh-DAPK1 was constructed to target DAPK1 by shRNA design tools (http://rnaidesigner.thermofisher.com/rnaiexpress/). Lentiviral-delivered specific sh-DAPK1 and sh-Con plasmids were packaged by Hanbio (Shanghai, China). The sequences of miR-Con (5'-ACGUGGUGUAAUAUUGGCCCCGA-3') and miR-361 (5'-UUAUCAGCAAUCUCCAGGGGUAC-3') were obtained using online predict software miRanda-mirSVR (http://www.microrna.org) and were synthesized by RiboBio (Guangzhou, China). The wild-type (WT) or mutant-type (Mut) 3'-UTR of DAPK1 were inserted into the multiple cloning sites of the luciferase-expressing pMIR-REPORT vector (Ambion; Thermo Fisher Scientific, Inc.). DAPK1 overexpressed plasmids (vector-DAPK1) were purchased from GeneCopoeia, Inc. (Rockville, MD, USA). All of the vectors were transfected into podocytes using Lipofectamine 2000 (Invitrogen; Thermo Fisher Scientific, Inc., Waltham, MA, USA) according to the manufacturer's protocols.

RT-qPCR

RT-qPCR for miRs: total RNA was extracted using the miRNeasy Mini Kit (Qiagen, Inc., Valencia, CA, USA). TaqMan® RT kit and TaqMan® MicroRNA assay (Applied Biosystems) were used to detect miR-361 expression levels using Applied Biosystems 7300 Real-Time PCR System (Thermo Fisher Scientific, Inc.). miR-361 expression levels were calculated using the $2^{-\Delta\Delta Ct}$ method, as described previously (Livak and Schmittgen, 2001), and U6 was used as an internal control.

RT-qPCR for mRNA: Moloney murine leukemia virus reverse transcriptase (Invitrogen) was used to synthesize cDNA with 2 μg of total RNA according to the manufacturer's protocol. Real-time PCR was performed using Applied Biosystems 7300 System with the TaqMan Universal PCR Master Mix (Thermo Fisher Scientific, Inc.). mRNA expression levels were calculated using the $2^{-\Delta\Delta Ct}$ method (Livak and

Schmittgen, 2001), and glyceraldehyde-3-phosphate dehydrogenase (GAPDH) served as the internal control. The primers were used as follows: DAPK1: Forward 5'-CGAGGTGATGGTGTATGGTG-3' and Reverse 5'-CTGTGCTTTGCTGGTGGA-3'; TNF-α: forward 5'-CTACCTTGTTGCCTCCTCTTT-3' and reverse 5'-GAGCAGAGGTTCAGTGATGTAG-3'; IL-1β: Forward 5'-ATGGGCAACCACTTACCTATTT-3' and Reverse 5'-GTTCTAGAGAGTGCTGCCTAATG-3'; IL-6: forward 5'-GTCTGTAGCTCATTCTGCTCTG-3' and reverse 5'-GAAGGCAACTGGATGGAAGTA-3'; GAPDH: forward 5'-GCACCGTCAAGCTGAGAAC-3' and reverse 5'-TGGTGAAGACGCCAGTGGA-3'.

Western blotting

Western blotting procedures were performed as previously described (Yu et al., 2018). The primary antibodies for DAPK1 (cat. no: sc-136286; dilution: 1: 1,000) and synaptopodin (cat. no: GTX39067, dilution: 1:500) were purchased from Santa Cruz Biotechnology (Santa Cruz, CA, USA) and GeneTex (San Antonio, TX, USA). Horseradish peroxidase-conjugated secondary antibody was obtained from Santa Cruz Biotechnology, Inc. (Dallas, TX, USA). Protein bands were visualized using an enhanced chemiluminescence kit (Thermo Fisher Scientific, Inc.). Signals were analyzed with Quantity One® software version 4.5 (Bio Rad Laboratories, Inc., Hercules, CA, USA). Anti-β-actin (cat. no. sc-130065; dilution: 1: 2,000; Santa Cruz Biotechnology) was used as the control antibody.

Enzyme-linked immunosorbent assay (ELISA)

The levels of tumor necrosis factor α (TNF-α), interleukin-1β (IL-1β) and interleukin 6 (IL-6) in the supernatant of cultured podocytes were measured by ELISA kit (Elabscience Biotechnology Co., Ltd, Wuhan, China). MDA level in the supernatant was detected using a commercial kit from the Nanjing Jiancheng Bioengineering Institute (Nanjing, China). 8-hydroxy-2'-deoxyguanosine (8-OHdG) was measured using a DNA damage ELISA kit (Enzo Life Sciences, Farmingdale, NY), according to the manufacturer's instructions.

Caspase-3 activity assay

Podocytes were lysated by NP-40 buffer, and the supernatant was collected for assay. In brief, 20 μl of cell lysate incubated with anti-caspase-3 antibody (cat.no: sc 7272; dilution, 1:200; Santa Cruz Biotechnology, Santa Cruz, CA, USA) at 37°C for 1 h. The immunocomplexes were then incubated with peptide substrate (2 μl of 10 mM acetyl-Asp-Glu-Val-Asp-p-nitroanilide) in assay buffer (100 mM Hepes, pH7.5, 20% v/v glycerol, 5 mM dithiothreitol, and 0.5 mM EDTA) for 2 h at 37°C. The release of p-nitroaniline was measured at 405 nm using an ELISA reader (MD SpectraMax M5; Molecular Devices, LLC, Sunnyvale, CA, USA).

Luciferase reporter gene assay

The wild-type (WT) and mutant-type (Mut) 3'-UTR of DAPK1 were inserted into the multiple cloning sites of the luciferase-expressing pMIR-REPORT vector (Ambion; Thermo Fisher Scientific, Inc., Waltham, MA, USA). After co-transfection with miR-Con or miR-361 combined with WT or Mut 3'-UTR of DAPK1 for 48 h, the luciferase activity was measured using a luciferase reporter assay kit (Promega Corporation, Madison, WI, USA) according to the manufacturer's protocols.

Animal experiments

Twelve week old male db/db mice and their normal littermates (db/m) were obtained from the SLAC Laboratory (Shanghai, China). Mice were fed under standard laboratory conditions with a temperature-controlled environment (temperature, 25±2°C; humidity, 60±5%), an artificial 12-h light/dark cycle. Mice were given free access to food and water and acclimated to the environment for one week prior to experimentation. Mice were divided into four groups (n=6 in each group): db/m group; db/db group; Agomir-miR-361 group (db/db mice received miR-361 agomir treatment); Agomir-Con group (db/db mice received Agomir-Con treatment). miR-361 agomir was synthesized by RiboBio Co., Ltd., Guangzhou, China. db/db mice were administrated with tail-vein injection (20 nM/0.1 mL) for 6 weeks (twice/week). After miR-361 agomir administration for 6 weeks, mice were sacrificed with euthanasia via an intravenous injection of sodium pentobarbital (200 mg/kg; Sigma-Aldrich; Merck KGaA, Germany). The animal experiment was approved by the Ethics Committee of the Linyi Central Hospital, Shandong Province, China. Animal research, including feeding, anesthesia with intraperitoneal injection of sodium pentobarbital (40 mg/kg; Sigma-Aldrich; Merck KGaA, Germany), sacrifice and specimen collection, conformed to the Animal Research: Reporting *In Vivo* Experiments guidelines 2.0 (Percie du Sert and Ahluwalia, 2020).

Biochemical parameters and GFR

Fasting blood glucose (FBG; Roche), serum insulin (Elabscience Biotechnology Co.,Ltd., Wuhan, China), plasma creatinine (Cre; BIOSINO, Biotechnology Co.,Ltd., Beijing, China), urinary albumin, and urinary albumin to creatinine ratio (ACR; BIOSINO, Biotechnology Co.,Ltd., Beijing, China) were measured using commercial kits according to the manufacturer's protocols. The insulin resistance index was analyzed as described previously (Chen and Liu, 2019). GFR was measured at the end of the experiment as described previously (Qi et al., 2004).

Histologic examination and immunohistochemical (IHC) staining

Podocyte counting in glomerulus was detected by WT-1 nuclear staining as described previously (Zhang et al., 2017). After fixation with 4% formalin at room temperature for 24 h, kidneys were embedded with paraffin and stained with hematoxylin & eosin (H&E) kit according to standard histological procedures of the manufacturer (Beyotime Institute of Biotechnology, Haimen, China). Masson's trichrome staining and interstitial fibrosis score were performed as described previously (Zhang et al., 2010). H&E and Masson's trichrome staining was visualized with an optical microscope (Olympus BX53, Japan). DAPK1 (cat. no: sc-136286; dilution: 1: 50) was used to detect DAPK1 protein expression in the kidney. IHC staining was performed as described previously (Shi et al., 2012).

Statistical analysis

Data are presented as the mean±standard deviation. Statistical analysis was performed using GraphPad Prism Version 7.0 (GraphPad Software, Inc., La Jolla, CA, USA). A Student's t-test was used to analyze the differences between the two groups. Differences between multiple groups were analyzed by one-way analysis of variance, followed by a post-hoc Tukey test. $p<0.05$ was considered to indicate a statistically significant difference.

Results

HG exposure down-regulates DAPK1 in podocytes

To determine the roles of DAPK1 on HG-evoked podocyte damage, we first detected the mRNA and protein expression levels of DAPK1 in podocytes in response to HG stimulation, and our findings corroborated a significant increase in DAPK1 mRNA (Fig. 1A) and protein (Fig. 1B) expression levels of HG-exposed podocyte compared with that of NG-treated podocytes. Furthermore, specific shRNA was designed to silence the expression of DAPK1. Transfection with sh-DAPK1 into podocytes resulted in a significant decrease in DAPK1 mRNA (Fig. 1C) and protein (Fig. 1D) expression.

DAPK1 silencing alleviates HG-caused podocyte growth inhibition, apoptosis and depletion

Further functional assay substantiated that HG stimulation impeded the growth of podocytes, while DAPK1 knockdown by specific shRNA relieved HG-induced proliferative inhibition (Fig. 2A). TUNEL staining revealed that HG incubation led to a significant increase in the number of TUNEL positive cells. However, HG-triggered apoptosis was significantly

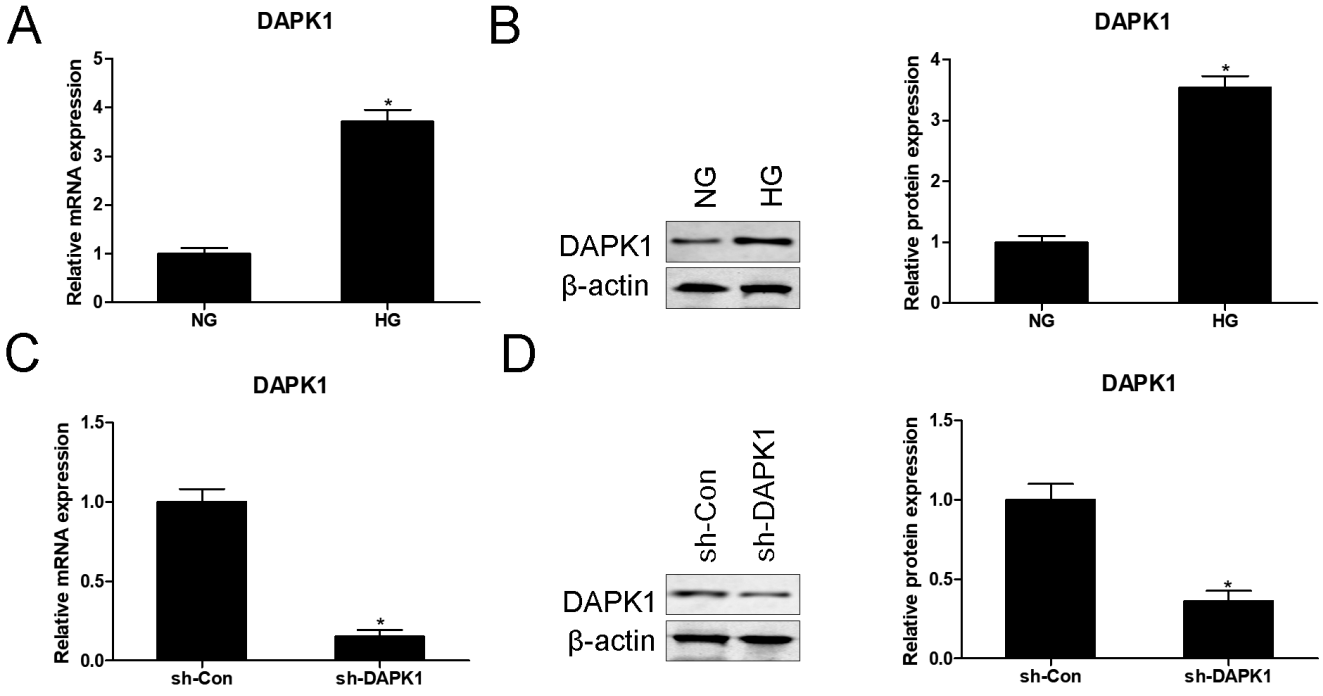

Fig. 1. HG exposure down-regulates DAPK1 in podocytes. After exposure podocyte to HG for 48 h, mRNA **(A)** and protein **(B)** expression levels of DAPK1 were monitored using RT-qPCR and western blotting, respectively. After transfection with sh-Con or sh-DAPK1 into podocytes for 48 h, mRNA **(C)** and protein **(D)** expression levels of DAPK1 were monitored using RT-qPCR and western blotting, respectively. N=3 in each group. * P<0.05.

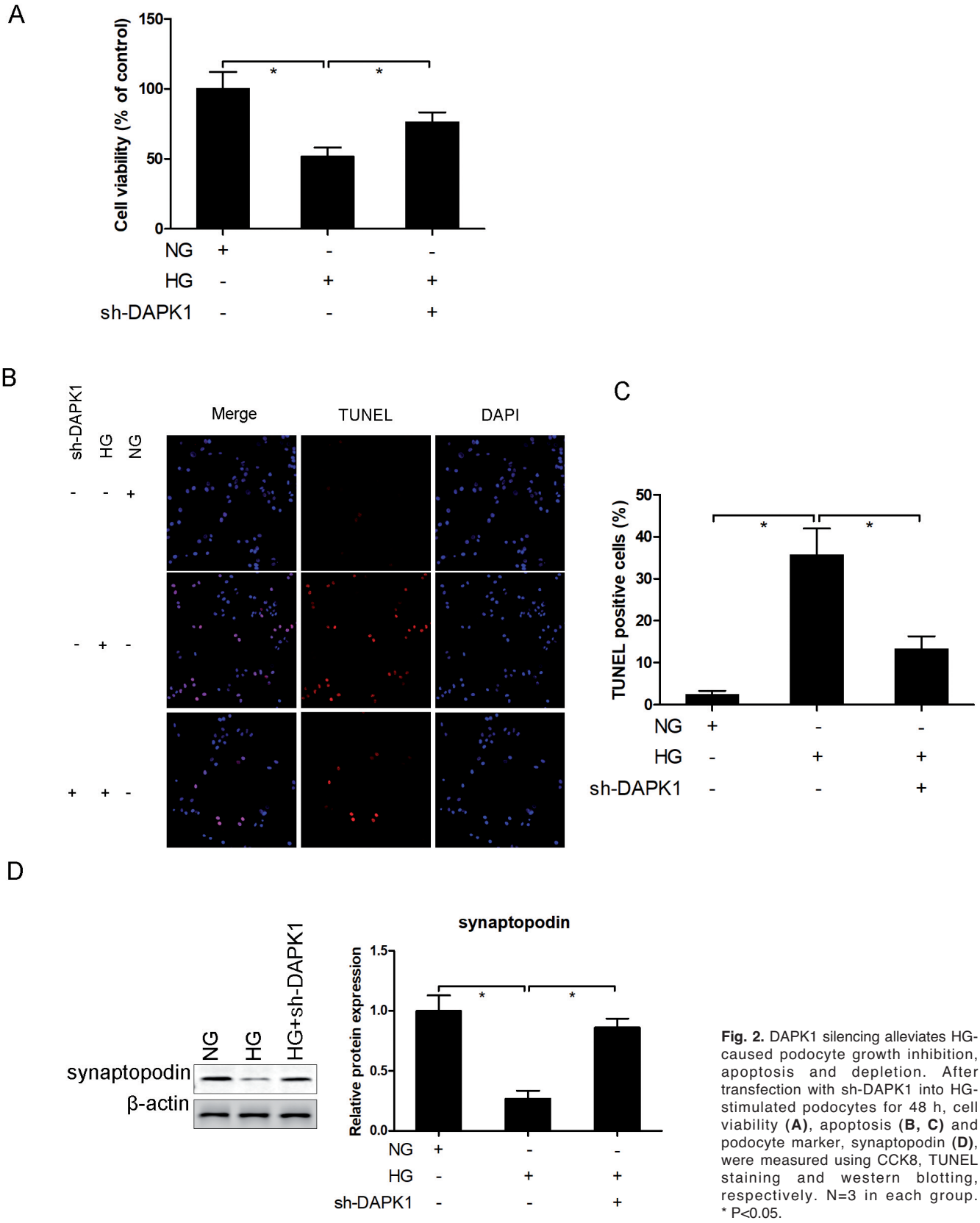

Fig. 2. DAPK1 silencing alleviates HG-caused podocyte growth inhibition, apoptosis and depletion. After transfection with sh-DAPK1 into HG-stimulated podocytes for 48 h, cell viability **(A)**, apoptosis **(B, C)** and podocyte marker, synaptopodin **(D)**, were measured using CCK8, TUNEL staining and western blotting, respectively. N=3 in each group. * P<0.05.

attenuated by sh-DAPK1 transfection (Fig. 2B,C). Additionally, HG administration restrained the protein expression of synaptopodin, which is a biomarker of podocytes and down-regulates in numerous kidney diseases and podocyte injury (Yu et al., 2016), while knockdown of DAPK1 reversed HG-induced down-regulation of synaptopodin protein expression in podocytes (Fig. 2D).

Knockdown of DAPK1 overturns HG-induced inflammatory response in podocytes

An inflammatory response is commonly accompanied with podocyte damage under HG conditions (Shi et al., 2016; Zhan et al., 2018). Herein, the effect of sh-DAPK1 transfection on HG-induced inflammation in podocytes was also investigated. In parallel with previous studies (Shi et al., 2016; Zhan et al., 2018), our results also validated that HG stimulation facilitated the secretion (Fig. 3A-C) and transcription (Fig. 3D-F) of inflammatory cytokines, including TNF-α, IL-1β and IL-6. However, HG-induced up-regulation of TNF-α, IL-1β and IL-6 levels in podocytes was markedly attenuated by sh-DAPK1 transfection.

HG-induced DNA damage and membrane damage in podocytes are neutralized by sh-DAPK1 transfection

We also investigated the effect of DAPK1 on HG-induced cellular DNA damage via evaluating the yield of 8-OHdG in cell supernatant liquid. HG stimulation increases the release of 8-OHdG , which is a biomarker to reflect the degree of DNA oxidative damage (Rai et al., 2015). However, knockdown of DAPK1 counteracted HG-induced up-regulation of the 8-OHdG level (Fig. 4A). We also discovered that HG treatment potentiated the release of MDA, which is a lipid peroxidation product and a marker of cell membrane damage (Whaley-Connell et al., 2006). Simultaneously, sh-DAPK1 transfection also counteracted HG-induced up-regulation of the MDA level in podocytes (Fig. 4B). As shown in Fig. 4C, exposure of podocytes to HG elevated the production of pro-apoptotic marker caspase3. Nevertheless, sh-DAPK1 transfection reversed HG-induced up-regulation of the caspase3 level in podocytes.

miR-361 directly targets DAPK1

To further elucidate the potential pathway in HG-induced podocyte damage via targeting DAPK1, we focused on miRs, which are widely studied as post-transcriptional regulators to repress the protein expression of target genes (Baek et al., 2008). Using the on-line bioinformatics algorithm (miRanda-mirSVR; http://www.microrna.org), we found that miR-361 was able to target the 3'-UTR of DAPK1 via complementary base pairing (Fig. 5A). Luciferase reporter gene assay

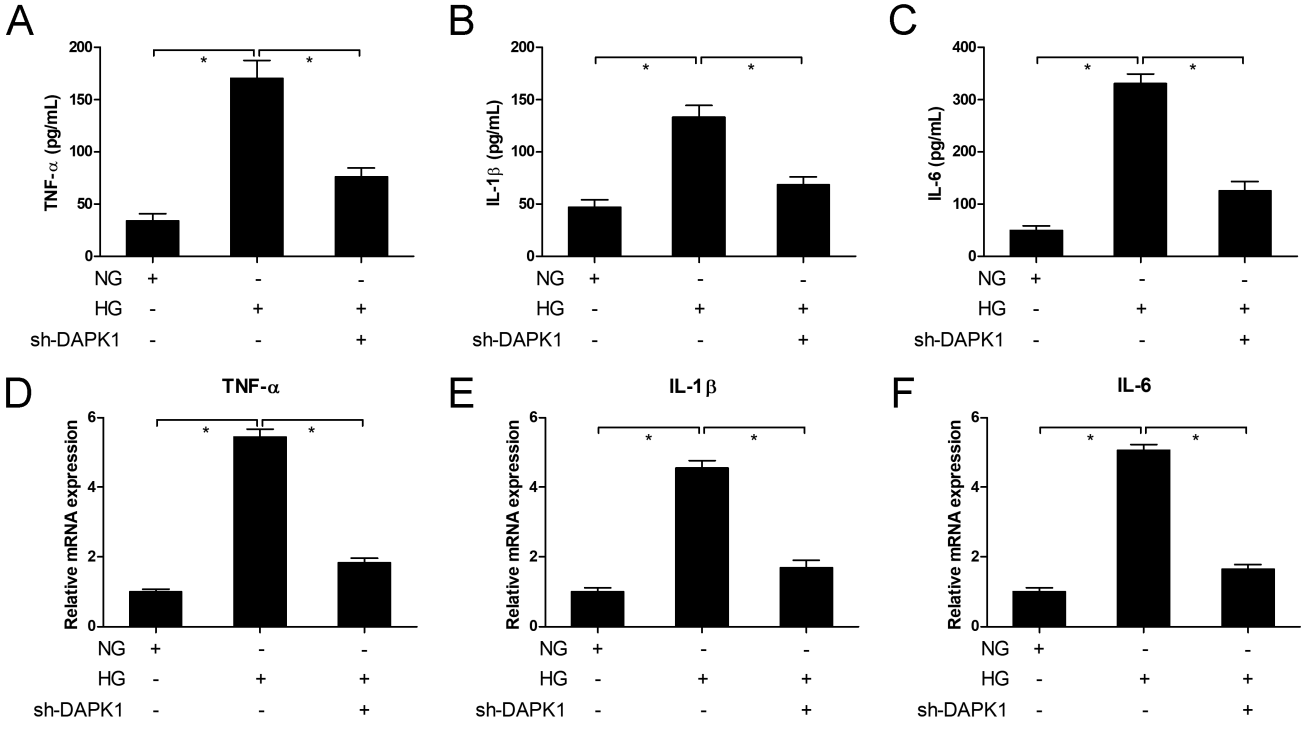

Fig. 3. The knockdown of DAPK1 overturns HG-induced inflammatory response in podocytes. After transfection with sh-DAPK1 into HG-stimulated podocytes for 48 h, the secretion **(A-C)** in the supernatant liquid and gene expression **(D-F)** of inflammatory cytokines, including TNF-α, IL-1β and IL-6, were measured using ELISA assays and RT-qPCR, respectively. N=3 in each group. * P<0.05.

was also performed to validate a direct association between miR-361 and DAPK1. WT or Mut 3'-UTR of DAPK1 was cloned into the luciferase reporter plasmid, which was co-transfected with miR-Con or miR-361 mimics into podocytes, and the results demonstrated that miR-361 mimics transfection led to a significant declined luciferase activity in podocytes containing WT 3'-UTR of DAPK1 (Fig. 5B). However, miR-361 mimic transfection had no obvious effect on luciferase activity in podocytes containing Mut 3'-UTR of DAPK1 (Fig. 5B).

Overexpression of DAPK1 counteracts the cytoprotection of miR-361 in HG-stimulated podocytes

Firstly, we found that the expression of miR-361 was significantly suppressed in HG-stimulated podocytes compared with NG-treated podocytes (Fig. 6A). Additionally, the protein expression of DAPK1 in podocytes was dramatically down-regulated by miR-361 mimic transfection compared with the control group (Fig. 6B). HG incubation increased DAPK1 expression, which was weakened after transfection with miR-361 mimics in podocytes (Fig. 6C). These findings suggest that miR-361 can directly down-regulate DAPK1 protein expression via post-transcriptional repression. Simultaneously, we found that the protective effect of miR-361 on HG-induced DAN damage (Fig. 6D) and cell membrane damage (Fig. 6E) was revoked by DAPK1 gain-of-function in podocytes. Furthermore, the anti-apoptotic effect of miR-361 on podocytes, reflecting that down-regulation of caspase3 production (Fig. 6F) and apoptotic cell proportion (Fig. 6G), in response to HG stimulation was attenuated by DAPK1 plasmid transfection.

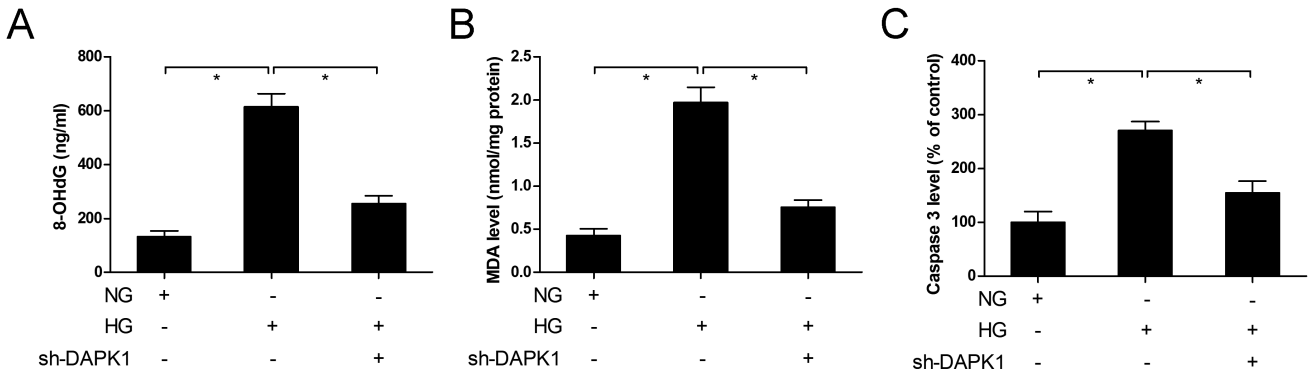

Fig. 4. HG-induced DNA damage and membrane damage in podocytes are neutralized by sh-DAPK1 transfection. After transfection with sh-DAPK1 into HG-stimulated podocytes for 48 h, DNA damage was evaluated using the yield of 8-OHdG in cell supernatant liquid **(A)**; MDA **(B)** and caspase3 **(C)** levels were measured using ELISA assays. N=3 in each group. * P<0.05.

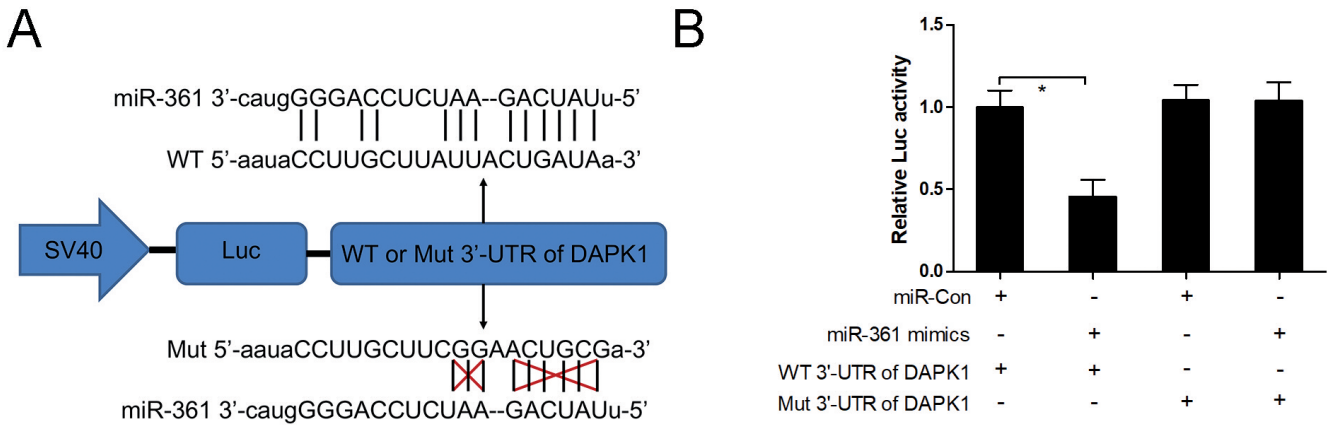

Fig. 5. miR-361 directly targets DAPK1. Using the on-line bioinformatics algorithm (miRanda-mirSVR; http://www.microrna.org), we found that miR-361 was able to target the 3'-UTR of DAPK1 via complementary base pairing **(A)**. After WT or Mut 3'-UTR of DAPK1 was cloned into the luciferase reporter plasmid and co-transfected with miR-Con or miR-361 mimics into podocytes, luciferase reporter gene assay was also performed to validate a direct association between miR-361 and DAPK1 **(B)**. N=3 in each group. * P<0.05.

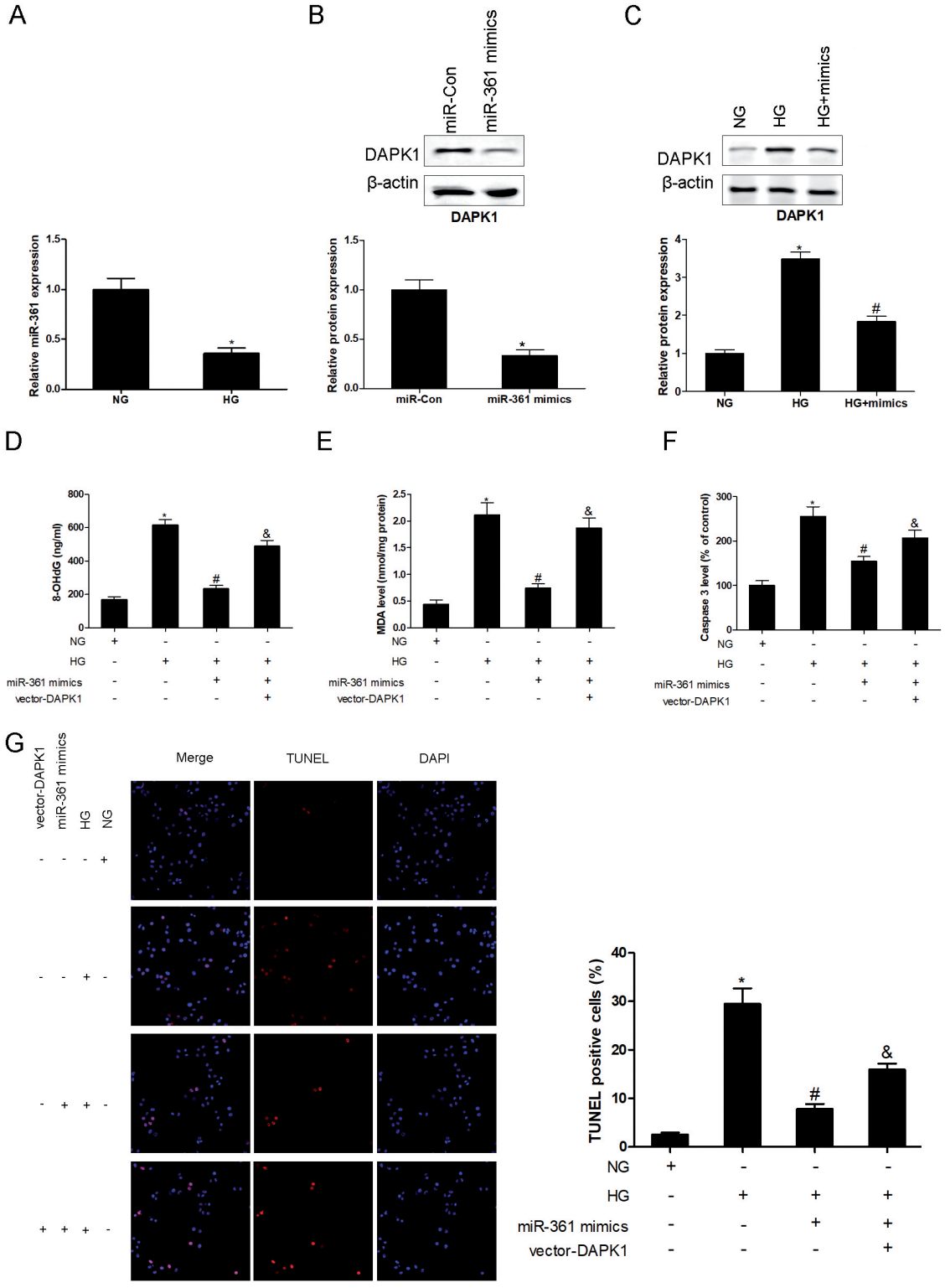

Fig. 6. Overexpression of DAPK1 counteracts the cytoprotection of miR-361 in HG-stimulated podocytes. The expression of miR-361 was measured in podocyte exposure to HG using RT-qPCR **(A)**. After transfection with miR-361 mimics into podocytes for 48 h, the protein expression levels of DAPK1 were monitored using western blotting **(B)**. After co-transfection with miR-361 mimics and vector-DAPK1 into HG-stimulated podocytes for 48 h, the protein expression levels of DAPK1 were monitored using western blotting **(C)**. After transfection with miR-361 mimics into HG-stimulated podocytes for 48 h, 8-OHdG **(D)**, MDA **(E)** and caspase3 **(F)** in cell supernatant liquid were measured to evaluate HG-induced podocyte damage; cell apoptosis was measured using TUNEL staining **(G)**. * P<0.05 compared with NG group; # P<0.05 compared with HG group; & P<0.05 compared with HG+miR-361 mimics group.

Overexpression of miR-361 alleviates renal damage in diabetic mice

To investigate whether up-regulation of miR-361 protects against hyperglycemia-induced renal damage, miR-361 agomir was administrated by tail intravenous injection in db/db diabetic mice. Our study demonstrated that miR-361 expression decreased in the kidney of db/db diabetic mice. However, miR-361 expression was immensely elevated in response to miR-361 agomir administration (Fig. 7A). miR-361 agomir administration had no obvious effect to reverse the increase in FBG and serum insulin in db/db diabetic mice (Fig. 7B,C). Interestingly, miR-361 agomir treatment significantly alleviated insulin resistance index (9.63±0.78) compared with that of in the untreated (14.29±1.38) or agomir-Con-treated db/db (15.82±1.71) mice (Fig. 7D). We also found that miR-361 agomir treatment significantly improved renal filtration function in db/db diabetic mice, reflecting that reversed hyperglycemia-induced increase in plasma Cre (0.42±0.03 mg/dl to 0.29±0.01 mg/dl; Fig. 7E), urinary albumin excretion (203.57±17.30 μg/l to 135.03±7.70 μg/l; Fig. 7F) and ACR (244.33±18.78 μg/mg to 158.33±14.38 μg/mg; Fig. 7G) and decrease in GFR (0.15±0.01 ml/min to 0.20±0.01 ml/min; Fig. 7H). Podocyte counting in glomerulus by WT-1 nuclear staining showed that reduction of podocyte number (11.66±2.05) in the glomerulus of db/db mice was significantly increased (29.33±2.86) after miR-361 agomir administration (Fig. 7I).

miR-361 agomir attenuates tubular atrophy and interstitial fibrosis in diabetic mice

Histologic examination by H&E staining and Masson's trichrome staining were performed to evaluate the protective effect of hyperglycemia-induced tubular

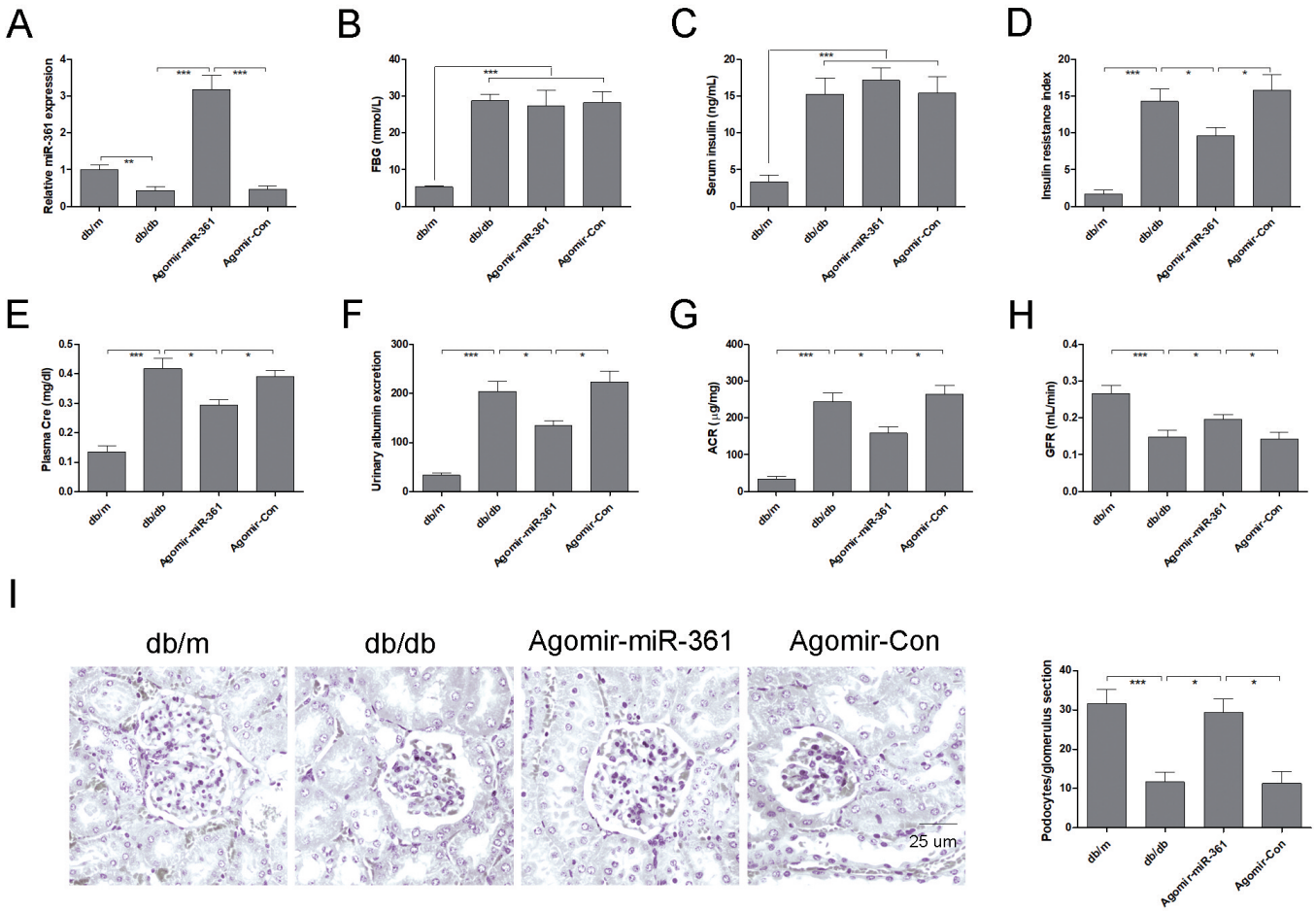

Fig. 7. Overexpression of miR-361 alleviates renal damage in diabetic mice. miR-361 expression was measured using RT-qPCR in the kidney of db/db mice in response to miR-361 agomir administration **(A)**. FBG **(B)**, serum insulin **(C)**, insulin resistance index **(D)**, plasma Cre **(E)**, urinary albumin excretion **(F)**, ACR **(G)** and GFR **(H)** were measured to evaluate the physiological and renal function of db/db mice in response to miR-361 agomir administration. Podocyte counting in glomerulus was detected by WT-1 nuclear staining (I). * P<0.05; ** P<0.01; *** P<0.001.

and interstitial damage in diabetic mice. As shown in Fig. 8A,B, severe tubular atrophy (Fig. 8A) and collagen deposition (blue staining in Fig. 8B) were observed in the kidney of db/db mice. However, miR-361 agomir markedly attenuated tubular pathological change in db/db mice (Fig. 8A). Semiquantitative scoring also confirmed that interstitial fibrosis in db/db mice was reversed by the treatment of miR-361 agomir (Fig. 8B).

miR-361 agomir down-regulates DAPK1 expression in the kidney of db/db mice

To determine the inhibitory action of miR-361 on DAPK1 *in vivo*, western blot and IHC staining were performed to analyze DAPK1 protein expression in the kidney of db/db mice afer miR-361 agomir treatment. As shown in Fig. 9A,B, a significant increase in DAPK1 protein expression occurred in the kidney of db/db mice as detected by western blot, while miR-361 agomir treatment significantly down-regulated DAPK1 protein expression in the kidney of db/db mice. Moreover, IHC staining also revealed that miR-361 agomir treatment obviously weakened DAPK1 protein expression in in the kidney of db/db mice (Fig. 9C).

Discussion

DAPK1 is originally identified in interferon-γ-induced apoptosis in HeLa cells (Deiss et al., 1995). Recently, abundant DAPK1 expression has been observed in the brain tissues and implicated in the pathogenesis of neurological diseases, including stroke, epilepsy and Alzheimer's disease (Singh et al., 2016; Wang et al., 2017). Accumulative evidence manifests that DAPK1 is up-regulated in response to noxious stimulus (Li et al., 2017; Xiong et al., 2018). For instance, ischemia-reperfusion (I/R) elevates DAPK1 expression in mouse N2a cells, as well as aggravating apoptosis in a time-dependent manner (Xiong et al., 2018). The up-regulation of DAPK1 is reported in the ovarian granulosa cells from the rat model with polycystic ovary syndrome (Li et al., 2017). Mechanically, the phosphorylation activity of DAPK1, as a Ca2+/calmodulin-dependent serine/threonine protein kinase, contributes to TNF-α, caspase and p53-mediated apoptosis (Singh et al., 2016; Wang et al.,

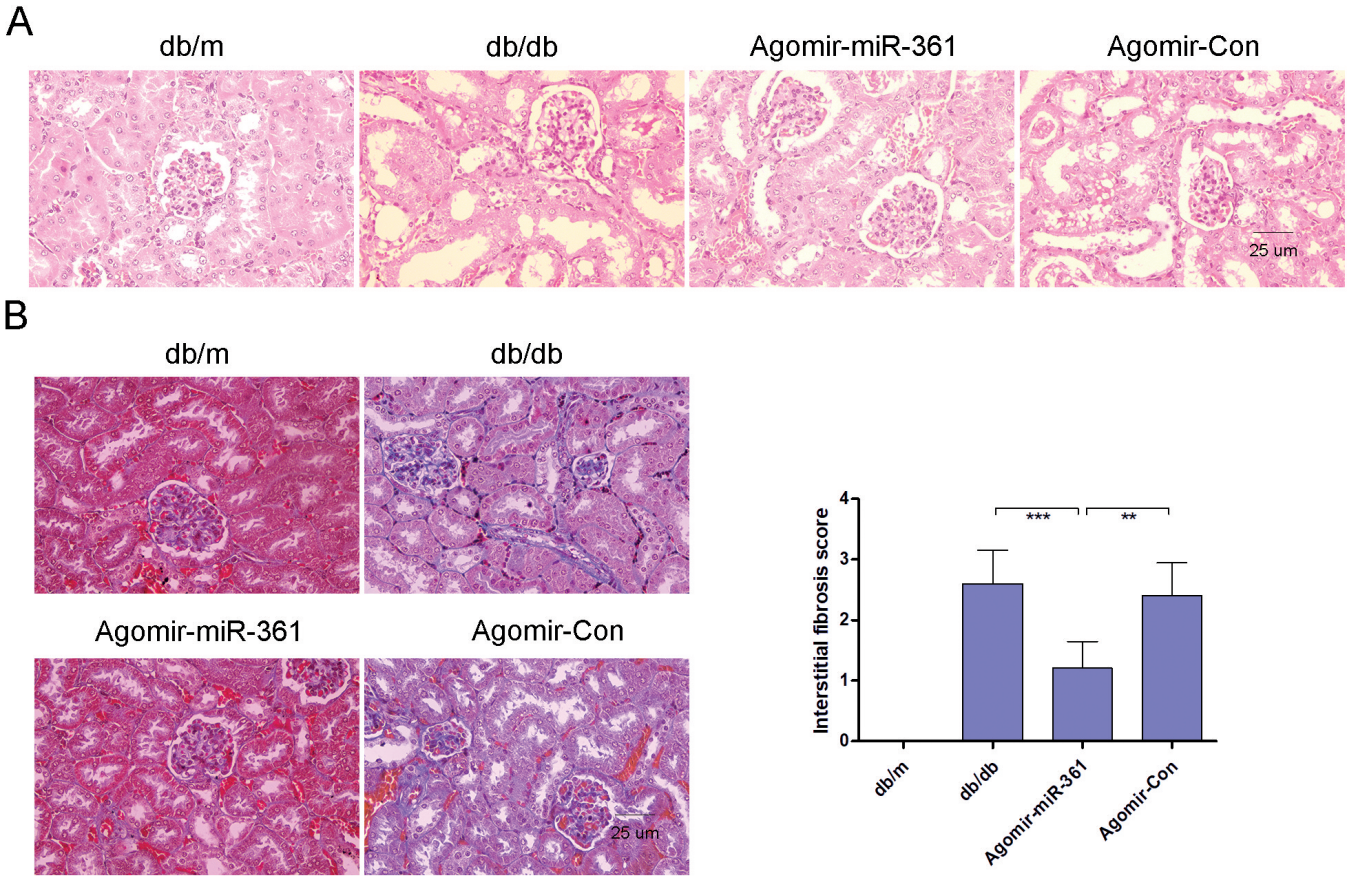

Fig. 8. miR-361 agomir attenuates tubular atrophy and interstitial fibrosis in diabetic mice. Histologic examination was evaluated by H&E staining **(A)** and Masson's trichrome staining with semiquantitative scoring **(B)**. ** P<0.01; *** P<0.001.

2017).

In the present study, the over-activation of DAPK1 was triggered by HG stimulation in podocytes and kidneys. However, knockdown of DAPK1 attenuated HG-triggered growth inhibition, apoptosis, DNA damage and cell membrane damage in podocytes. These findings suggested that DAPK1 played a crucial role in unraveling the mechanisms of HG-evoked podocyte apoptosis. White et al corroborates that DAPK1 activation is associated with lung endothelial cell apoptosis during ischemic acute kidney injury (White et al., 2012). Of interest, our results highlighted that up-regulation of DAPK1 was implicated in HG-evoked inflammatory response and apoptosis in podocytes.

Although the pathogenic mechanism of HG-induced podocyte apoptosis is complicated, overwhelming evidence indicates that miRs as post-transcriptional regulators participate in this pathological process via modulating multiple target genes (Lin et al., 2014; Xu et al., 2017; Fu et al., 2019). For example, miR-15b-5p, miR-21, miR-27a and miR-

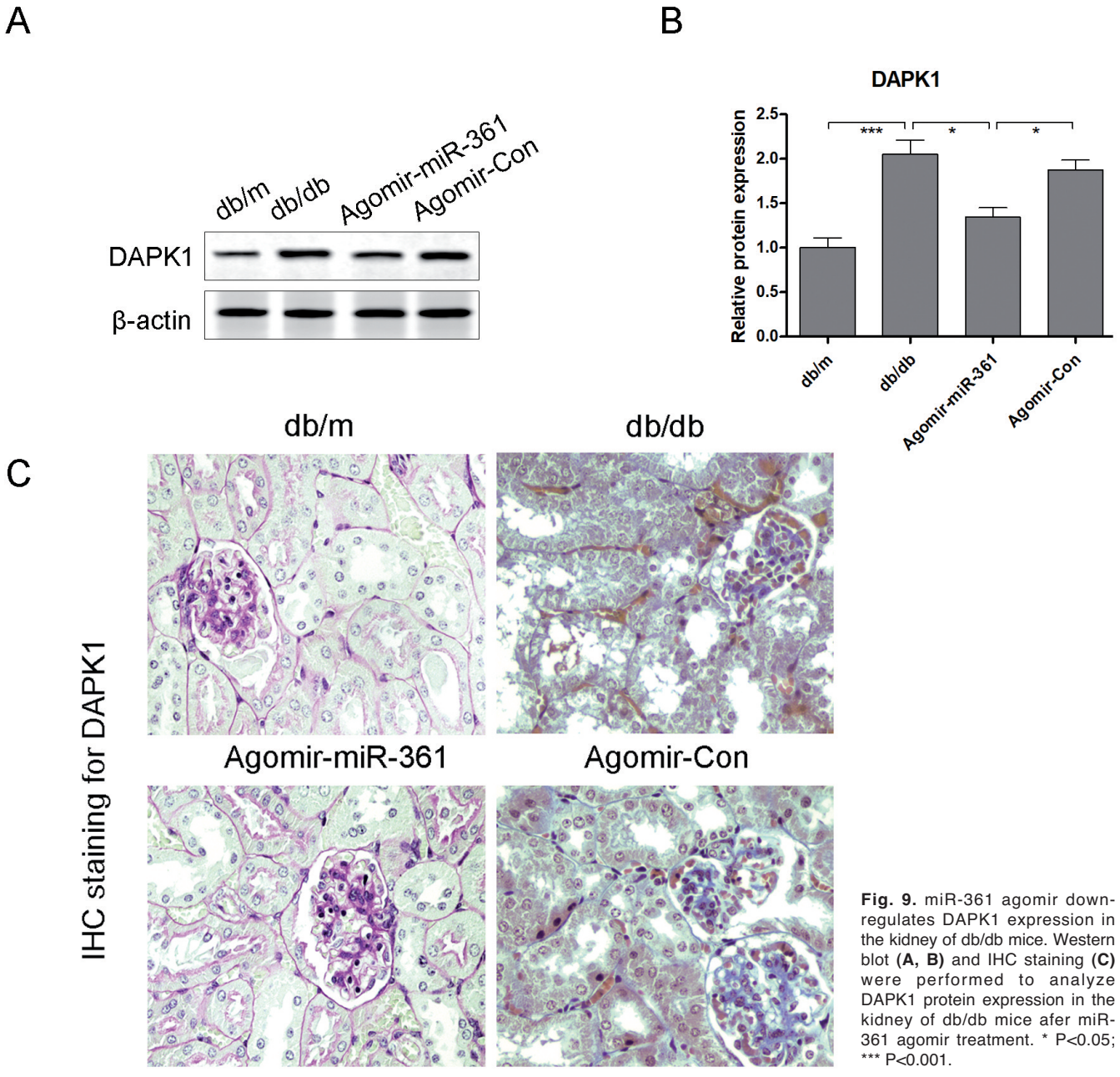

Fig. 9. miR-361 agomir down-regulates DAPK1 expression in the kidney of db/db mice. Western blot **(A, B)** and IHC staining **(C)** were performed to analyze DAPK1 protein expression in the kidney of db/db mice afer miR-361 agomir treatment. * P<0.05; *** P<0.001.

29a show a direct correlation with podocyte injuries through affecting their target genes, which are associated with inflammation, autophagy and apoptosis (Lin et al., 2014; Xu et al., 2017; Zhou et al., 2017; Fu et al., 2019). Previous study reveals that miR-361 is responsible for the dysfunction of mitochondrial homeostasis and apoptosis to accelerate myocardial infarction and heart failure (Wang et al., 2015). However, the biological effect of miR-361 on podocytes is still unclear. In our study, we established a miR-361 overexpressed podocyte, and the podocyte injury model was incubated by HG stimulation. Our findings illustrated a protective effect of overexpressed miR-361 on HG-induced podocyte dysfunction, including apoptosis, DNA damage and cell membrane damage. *In vivo*, miR-361 agomir protected against hyperglycemia-induced podocyte loss, tubular atrophy and interstitial fibrosis in the kidney of db/db mice. Moreover, miR-361 agomir inhibited the protein expression of DAPK1 in the kidney of db/db mice. These findings indicate that miR-361 agomir may be a prospective therapeutic drug to prevent hyperglycemia-induced renal dysfunction in diabetic mice. Inhibition of DAPK1 by miR-361 may represent a novel signaling pathway to ameliorate renal damage in diabetic mice.

In our study, it was revealed that DAPK1 was a direct target of miR-361. Transfection with miR-361 mimics into podocytes led to a significant decrease in the DAPK1 protein expression level. In addition, HG-evoked up-regulation of DAPK1 protein expression level in podocytes was counteracted by miR-361 mimic transfection. Intriguingly, overexpression of DAPK1 in HG-stimulated podocytes muted miR-361-mediated cytoprotection, including anti-apoptosis, resistance to DNA and membrane damage. These findings exhibited an almost completely opposite function between miR-361 and DAPK1 in the process of HG-induced podocyte damage. Previous studies document that miR-26a-5p, miR-98, miR-141-3p and miR-194-3p-modulated post-transcriptional repression of DAPK1 attenuates cell apoptosis, inflammation and dysfunction in different cell injury models (Li et al., 2017; Zhou et al., 2018; Wei et al., 2019; Zhai et al., 2019).

However, there are a few limitations to the present study. First, the security and adverse effects of miR-361 agomir have not been completely evaluated in diabetic mice. Second, the direct correlation between DAPK1 and apoptosis or inflammation in HG-treated podocytes has not been explored *in vitro*. Furthermore, miR-361 agomir administration as a potential gene therapy is uncertain in the clinical practice.

In conclusion, miR-361 overexpression antagonized HG-induced podocyte dysfunction and renal damage by targeting DAPK1. These findings presented a novel mechanism of HG-induced podocyte and renal damage, supporting the miR-361/DAPK1 signaling pathway that could be used as a potential therapeutic target for the treatment of DN.

Funding. This research received no specific grant from any funding agency in the public, commercial or not-for-profit sectors.

Disclosure of conflict of interest. The authors declare they have no competing interests.

Authors' contributions. Study design: G-W and X-Z; Literature research: G-W, H-Z, X-Z; Data acquisition and Data analysis: G-W, H-Z, X-Z; manuscript preparation: G-W, H-Z, X-Z; manuscript editing: G-W and X-Z; manuscript review: G-W, H-Z, X-Z; Cell experiments: G-W, H-Z, X-Z. Final approval of the version to be published: G-W, H-Z, X-Z.

References

Baek D., Villen J., Shin C., Camargo F.D., Gygi S.P. and Bartel D.P. (2008). The impact of micrornas on protein output. Nature 455, 64-71.

Chen S.H. and Liu X.N. (2019). MicroRNA-351 eases insulin resistance and liver gluconeogenesis via the PI3K/AKT pathway by inhibiting FLOT2 in mice of gestational diabetes mellitus. J. Cell. Mol. Med. 23, 5895-5906.

Chen Z., Chen Q., Huang J., Gong W., Zou Y., Zhang L., Liu P. and Huang H. (2018). CK2alpha promotes advanced glycation end products-induced expressions of fibronectin and intercellular adhesion molecule-1 via activating MRTF-a in glomerular mesangial cells. Biochem. Pharmacol. 148, 41-51.

Cui S.N., Chen L., Yang Y.Y., Wang Y.X., Li S.N., Zhou T., Xiao H.R., Qin L., Yang W., Yuan S.Y., Yao S.L. and Shang Y. (2019). Activation of death-associated protein kinase 1 promotes neutrophil apoptosis to accelerate inflammatory resolution in acute respiratory distress syndrome. Lab. Invest. 99, 1143-1156.

Dai H. Liu Q. and Liu B. (2017). Research progress on mechanism of podocyte depletion in diabetic nephropathy. J. Diabetes. Res. 2017, 2615286.

Deiss L.P., Feinstein E., Berissi H., Cohen O. and Kimchi A. (1995). Identification of a novel serine/threonine kinase and a novel 15-kd protein as potential mediators of the gamma interferon-induced cell death. Genes. Dev. 9, 15-30.

Fu Y., Wang C., Zhang D., Chu X., Zhang Y. and Li J. (2019). Mir-15b-5p ameliorated high glucose-induced podocyte injury through repressing apoptosis, oxidative stress, and inflammatory responses by targeting Sema3a. J. Cell. Physiol. 234, 20869-20878.

Huang K., Yu X., Yu Y., Zhang L., Cen Y. and Chu J. (2020). Long noncoding RNA MALAT1 promotes high glucose-induced inflammation and apoptosis of vascular endothelial cells by regulating mir-361-3p/SOCS3 axis. Int. J. Clin. Exp. Pathol. 13, 1243-1252.

Li D., Xu D., Xu Y., Chen L., Li C., Dai X., Zhang L. and Zheng L. (2017). MicroRNA-141-3p targets DAPK1 and inhibits apoptosis in rat ovarian granulosa cells. Cell. Biochem. Funct. 35, 197-201.

Liang H.F., Zhang X.Z., Liu B.G., Jia G.T. and Li W.L. (2017). Circular RNA circ-ABCB10 promotes breast cancer proliferation and progression through sponging miR-1271. Am. J. Cancer Res. 7, 1566-1576.

Lin C.L., Lee P.H., Hsu Y.C., Lei C.C., Ko J.Y., Chuang P.C., Huang Y.T., Wang S.Y., Wu S.L., Chen Y.S., Chiang W.C., Reiser J. and Wang F.S. (2014). MicroRNA-29a promotion of nephrin acetylation ameliorates hyperglycemia-induced podocyte dysfunction. J. Am.

Soc. Nephrol. 25, 1698-1709.

Livak K.J. and Schmittgen T.D. (2001). Analysis of relative gene expression data using real-time quantitative pcr and the 2(-delta delta c(t)) method. Methods 25, 402-408.

Mendes-Silva A.P., Pereira K.S., Tolentino-Araujo G.T., Nicolau Ede S., Silva-Ferreira C.M., Teixeira A.L. and Diniz B.S. (2016). Shared biologic pathways between alzheimer disease and major depression: A systematic review of microrna expression studies. Am. J. Geriatr. Psychiatry 24, 903-912.

Percie du Sert N. and Ahluwalia A. (2020). Reporting animal research: Explanation and elaboration for the arrive guidelines 2.0. PLoS. Biol. 18, e3000411.

Qi Z., Whitt I., Mehta A., Jin J., Zhao M., Harris R.C., Fogo A.B. and Breyer M.D. (2004). Serial determination of glomerular filtration rate in conscious mice using FITC-inulin clearance. Am. J. Physiol. Renal. Physiol. 286, F590-596.

Rai P., Singh T., Lederman R., Chawla A., Kumar D., Cheng K., Valecha G., Mathieson P.W., Saleem M.A., Malhotra A. and Singhal P.C. (2015). Hyperglycemia enhances kidney cell injury in hivan through down-regulation of vitamin d receptors. Cell. Signal. 27, 460-469.

Roscioni S.S., Heerspink H.J. and de Zeeuw D. (2014). The effect of raas blockade on the progression of diabetic nephropathy. Nat. Rev. Nephrol. 10, 77-87.

Shi T.J., Xiang Q., Zhang M.D., Tortoriello G., Hammarberg H., Mulder J., Fried K., Wagner L., Josephson A., Uhlén M., Harkany T. and Hökfelt T. (2012). Secretagogin is expressed in sensory cgrp neurons and in spinal cord of mouse and complements other calcium-binding proteins, with a note on rat and human. Mol. Pain. 8, 80.

Shi J.X., Wang Q.J., Li H. and Huang Q. (2016). Silencing of USP22 suppresses high glucose-induced apoptosis, ros production and inflammation in podocytes. Mol. Biosyst. 12, 1445-1456.

Singh P., Ravanan P. and Talwar P. (2016). Death associated protein kinase 1 (DAPK1): A regulator of apoptosis and autophagy. Front. Mol. Neurosci. 9, 46-46.

Thongchot S., Vidoni C., Ferraresi A., Loilome W., Yongvanit P., Namwat N. and Isidoro C. (2018). Dihydroartemisinin induces apoptosis and autophagy-dependent cell death in cholangiocarcinoma through a DAPK1-BECLIN1 pathway. Mol. Carcinog. 57, 1735-1750.

Wang K., Liu C.Y., Zhang X.J., Feng C., Zhou L.Y., Zhao Y. and Li P.F. (2015). Mir-361-regulated prohibitin inhibits mitochondrial fission and apoptosis and protects heart from ischemia injury. Cell. Death. Differ. 22, 1058-1068.

Wang S., Shi X., Li H., Pang P., Pei L., Shen H. and Lu Y. (2017). Dapk1 signaling pathways in stroke: From mechanisms to therapies. Mol. Neurobiol. 54, 4716-4722.

Wei R., Zhang L., Hu W., Wu J. and Zhang W. (2019). Long non-coding RNA AK038897 aggravates cerebral ischemia/reperfusion injury via acting as a ceRNA for miR-26a-5p to target DAPK1. Exp. neurol. 314, 100-110.

Whaley-Connell A.T., Chowdhury N.A., Hayden M.R., Stump C.S., Habibi J., Wiedmeyer C.E., Gallagher P.E., Tallant E.A., Cooper S.A., Link C.D., Ferrario C. and Sowers J.R. (2006). Oxidative stress and glomerular filtration barrier injury: Role of the renin-angiotensin system in the Ren2 transgenic rat. Am. J. Physiol. Renal. Physiol. 291, F1308-1314.

White L.E., Cui Y., Shelak C.M.F., Lie M.L. and Hassoun H.T. (2012). Lung endothelial cell apoptosis during ischemic acute kidney injury. Shock 38, 320-327.

Xiong W., Wu Y., Xian W., Song L., Hu L., Pan S., Liu M., Yao S., Pei L. and Shang Y. (2018). DAPK1-ERK signal mediates oxygen glucose deprivation reperfusion induced apoptosis in mouse N2a cells. J. Neurol. Sci. 387, 210-219.

Xu D. and Dong P. (2019). MicroRNA-361: A multifaceted player regulating tumor aggressiveness and tumor microenvironment formation. Cancers (Basel) 11, 1130.

Xu L., Fan Q., Wang X., Li L., Lu X., Yue Y., Cao X., Liu J., Zhao X. and Wang L. (2017). Ursolic acid improves podocyte injury caused by high glucose. Nephrol. Dial. Transplant. 32, 1285-1293.

Yu H., Kistler A., Faridi M.H., Meyer J.O., Tryniszewska B., Mehta D., Yue L., Dryer S. and Reiser J. (2016). Synaptopodin limits TRPC6 podocyte surface expression and attenuates proteinuria. J. Am. Soc. Nephrol. 27, 3308-3319.

Yu F.Y., Xie C.Q., Sun J.T., Peng W. and Huang X.W. (2018). Overexpressed mir-145 inhibits osteoclastogenesis in RANKL-induced bone marrow-derived macrophages and ovariectomized mice by regulation of SMAD3. Life Sci. 202, 11-20.

Zhai C.-L., Tang G.-M., Qian G., Hu H.-L., Wang S.-J., Yin D. and Zhang S. (2019). MicroRNA-98 attenuates cardiac ischemia-reperfusion injury through inhibiting DAPK1 expression. IUBMB life 71, 166-176.

Zhan X., Yan C., Chen Y., Wei X., Xiao J., Deng L., Yang Y., Qiu P. and Chen Q. (2018). Celastrol antagonizes high glucose-evoked podocyte injury, inflammation and insulin resistance by restoring the HO-1-mediated autophagy pathway. Mol. Immunol. 104, 61-68.

Zhang Y., Kong J., Deb D.K., Chang A. and Li Y.C. (2010). Vitamin D receptor attenuates renal fibrosis by suppressing the renin-angiotensin system. J. Am. Soc. Nephrol. 21, 966-973.

Zhang M.Z., Wang X., Yang H., Fogo A.B., Murphy B.J., Kaltenbach R., Cheng P., Zinker B. and Harris R.C. (2017). Lysophosphatidic acid receptor antagonism protects against diabetic nephropathy in a type 2 diabetic model. J. Am. Soc. Nephrol. 28, 3300-3311.

Zhao B., Li H., Liu J., Han P., Zhang C., Bai H., Yuan X., Wang X., Li L., Ma H., Jin X. and Chu Y. (2016). MicroRNA-23b targets ras GTPase-activating protein SH3 domain-binding protein 2 to alleviate fibrosis and albuminuria in diabetic nephropathy. J. Am. Soc. Nephrol. 27, 2597-2608.

Zhou Z., Wan J., Hou X., Geng J., Li X. and Bai X. (2017). MicroRNA-27a promotes podocyte injury via PPARγ-mediated β-catenin activation in diabetic nephropathy. Cell. Death. Dis. 8, e2658-e2658.

Zhou T., Zhong Y., Hu Y., Sun C., Wang Y. and Wang G. (2018). PM2.5 downregulates miR-194-3p and accelerates apoptosis in cigarette-inflamed bronchial epithelium by targeting death-associated protein kinase 1. Int. J. Chron. Obstruct. Pulmon. Dis. 13, 2339-2349.

Accepted July 16, 2021